JACS
JOURNAL OF THE AMERICAN CHEMICAL SOCIETY
Article
pubs.acs.org/JACS

Synthesis and Spectroscopy of PbSe Fused Quantum-Dot Dimers

Barbara K. Hughes,[†,‡] Jeffrey L. Blackburn,[†] Daniel Kroupa,[‡] Andrew Shabaev,[§] Steven C. Erwin,[∥] Alexander L. Efros,[∥] Arthur J. Nozik,[†,‡] Joseph M. Luther,[†] and Matthew C. Beard*[,†]

[†]National Renewable Energy Laboratory, Chemical and Material Sciences Center, Golden, Colorado 80401, United States
[‡]University of Colorado, Chemical and Biosciences Department, Boulder, Colorado 80309, United States
[§]George Mason University, Fairfax, Virginia 22030, United States
[∥]Center for Computational Materials Science, Naval Research Laboratory, Washington, D.C. 20375, United States

Supporting Information

ABSTRACT: We report the synthesis and characterization of Pb-chalcogenide fused quantum-dot (QD) dimer structures. The resulting QD dimers range in length from 6 to 16 nm and are produced by oriented attachment of single QD monomers with diameters of 3.1−7.8 nm. QD monomers with diameters exceeding about 5 nm appear to have the greatest affinity for QD dimer formation and, therefore, gave the greatest yields of fused structures. We find a new absorption feature in the first exciton QD dimer spectra and assign this to a splitting of the 8-fold degenerate 1S-level. The dimer splitting increases from 50 to 140 meV with decrease of the QD-monomer size, and we present a mechanism that accounts for this splitting. We also demonstrate the possibility of fusing two QDs with different sizes into a heterostructure.

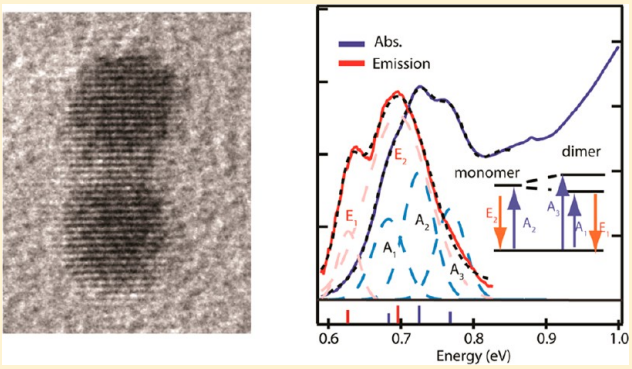

INTRODUCTION

In the past decade, semiconductor quantum dots (QDs) have demonstrated tremendous potential as nanoscale building blocks to form complex structures and morphologies via bottom-up synthesis and assembly approaches.[1−4] In addition to the applications that novel nanocrystal morphologies may enable, it is highly desirable to attain a more detailed fundamental understanding of the surface interactions and nanocrystal (NC)-assembly mechanisms that produce these structures. A better understanding of how to manipulate nanocrystal morphologies, QD surfaces,[5] stoichiometry,[5] and composition[6] is needed to control excited state dynamics and energy flow[7−9] for novel approaches to solar energy capture and usage. In this study, we describe a solution-based oriented attachment method for preparing fused dimer-like structures of semiconductor PbSe QDs (hereafter referred to as QD dimers) from colloidal solutions of already synthesized conventional PbSe QDs (hereafter referred to as QD monomers). We show that the QD dimer yields are strongly controlled by reaction conditions, surface stabilizers and initial QD-monomer size.

Oriented attachment in PbSe QDs has been the subject of numerous studies over the past few years,[1,2,10−13] ranging from cryo-TEM[10] studies to computational molecular dynamics.[12] The emerging view from these studies is that oriented attachment in PbSe QDs is driven by the reduction of surface energies[10,12] rather than strong dipole−dipole interactions. In one of the first reports of oriented attachment in the PbSe system, multidimensional structures of PbSe such as rods, wires, rings, and stars were prepared by manipulation of surface ligands.[1] PbSe QD monomers can be encouraged to fuse along exposed lattice facets to produce nanowires with lengths ranging from 3 to 30 μm, while the diameter is confined to that of the individual QD monomers. In Figure 1, we show QD monomers and various types of elongated structures produced in our laboratory following these principles in which the elongated structures (dimers, rods, and wires) consist of multiple fused QD monomers. The lattice plane along which QDs fuse can be manipulated by the choice of stabilizing surfactant, leading to a variety of nanowires, such as, zigzag, straight, and undulated.[1] Different surfactants stabilize different exposed facets and thus help determine the most reactive facet for subsequent fusion.[2] Hanrath and co-workers found that treating oleic acid passivated PbSe QDs with pyridine resulted in polymeric PbSe QD networks in which lattice fusion occurs in multiple directions. The resulting morphology was found to be QD-size-dependent, presumably correlated to differing exposed facets that occur for QDs of different size.[14] Recently, Evers et al. studied the formation of complex PbSe QD networks.[2] They varied the QD concentration, stabilizing ligand, and film drying temperature and found that, depending on the synthetic conditions, various PbSe QD networks could be produced, resulting in 1D or 2D semiconductors.

Received: December 30, 2013
Published: February 24, 2014

   dx.doi.org/10.1021/ja413026h | J. Am. Chem. Soc. 2014, 136, 4670−4679

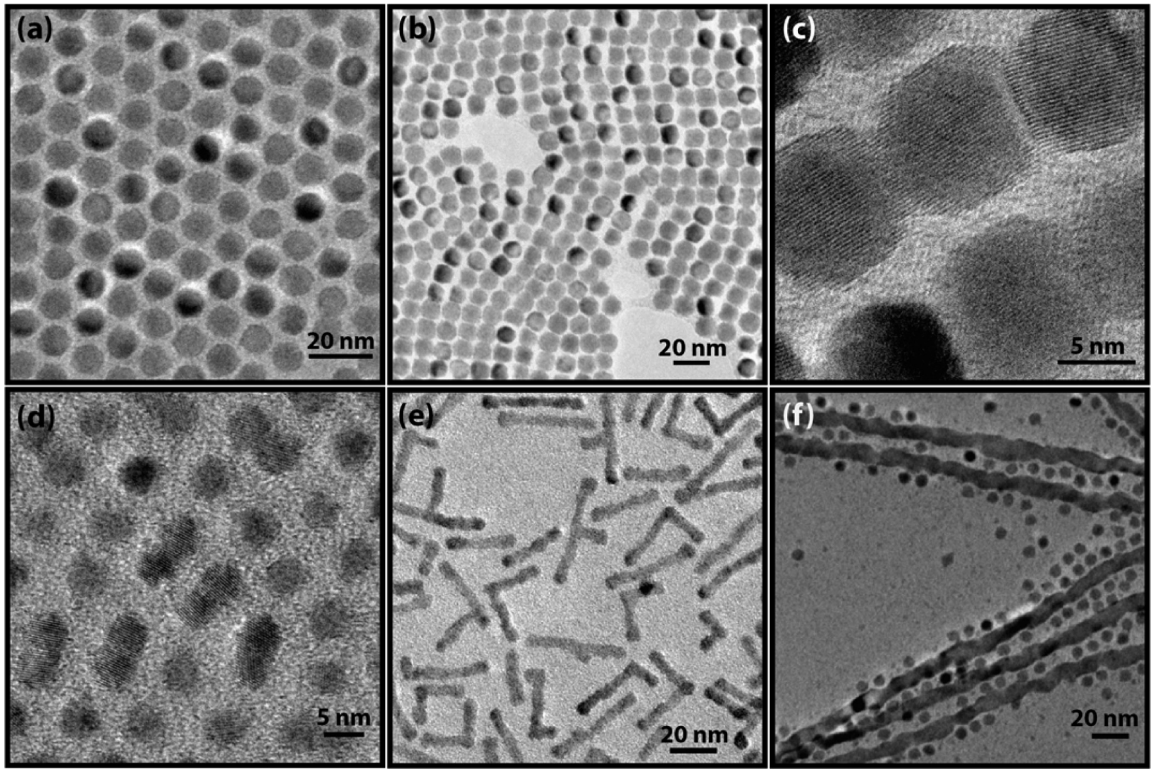

Figure 1. (a) TEM image of a hexagonal close packed array of separated "QD monomers". The separation is caused by hydrocarbon ligands attached to the surface after synthesis. Upon heating such monomers with additional surfactant, QDs associate such that the space between them is reduced along certain crystallographic directions (b). The packing also changes more toward a cubic assembly. (c) Initial stages of fused chains of QD monomers. Under controlled conditions, QD dimers (d), quantum rods (e), or quantum-wire (f) structures are formed.

In this work, we demonstrate that by controlling the growth time, temperature, and stabilizing ligand for the post-treatment of as-prepared QDs, the size of QD chains can be engineered to favor the formation of PbSe QD dimers as the predominant reaction product compared with larger QD oligomers. In contrast to a recently developed one-pot synthesis of PbSe quantum rods (QRs),[11] the present synthesis provides a unique approach that could enable greater control over QR length and structure by controlling the number of monomers that fuse to form into single crystalline chains. Additionally, our approach to preparing PbSe QD dimer structures demonstrates that QD monomers can be building blocks for more complex nanostructures via oriented attachment. Oriented attachment is emerging as a general synthetic strategy for producing a variety of functional nanostructures,[1,2,11,15,16] and our study provides insight into the mechanisms underlying oriented attachment and the nanoarchitectures that are possible using such bottom-up approaches to nanostructure synthesis.

We also study the optical transitions in QD dimer structures and find a unique splitting of the ground state exciton. This splitting is explained by the coupling between individual QDs in the dimer. Although the QDs are faceted polyhedrons, the coupling is calculated in a spherical approximation for 1S ground states assuming that each sphere is concentric with the QD polyhedron of the same volume as the sphere. The dimer is formed by two polyhedrons in contact at one of their facets. Accordingly, in our approximation, these two spheres overlap to form a lens-shaped region with a thickness proportional to the spheres radii. Finally, using both the experimental splittings and the spherical approximation, we can speculate about the possible shapes of individual QDs.

QD DIMER FORMATION AND YIELD

For a typical dimer synthesis, 50 mg of as-made QDs are first dispersed in a minimum amount of hexane. To this dispersion, 5 mL of 1-octadecene and 0.35 mL of oleic acid, $Pb(oleate)_2$, or oleylamine is added. The small amount of hexane is then removed by vacuum and gentle heating, and the remaining QD solution is heated to 150 °C for 1 h under N_2 and then cooled to room temperature and precipitated twice using a centrifuge and ethanol/hexane as the solvent pair. Standard (Schlenk and glovebox) air-free techniques are used throughout. TEM images show appreciable numbers of QD dimers in the sample depending on heating time and ligand moiety and concentration. With each of the ligands used here, excessive heating results in uncontrolled ripening as well as the formation of larger oligomeric material (trimers, tetramers, etc.) rather than the desired QD dimers.

We also developed an alternative method for synthesizing QD dimers with reduced reaction times and comparable yields by using a microwave reactor in which the temperature of the solution can be rapidly increased (and decreased) in a more-controlled manner.[17] For a typical microwave reaction, we utilized the previously mentioned quantities of reactants. The reactants are loaded into the reaction vessel after hexane has been removed from the solution. While we monitor both the temperature and the pressure, the reaction mixture is heated to 150 °C under vigorous stirring, at which point the temperature is held constant for 1 min 30 s prior to cooling to room temperature. The product from this reaction route is purified similarly as described above. QD dimers synthesized in this study were prepared by both synthetic methods with no appreciable differences in QD dimer quality or yield.

dx.doi.org/10.1021/ja413026h | J. Am. Chem. Soc. 2014, 136, 4670−4679

PbSe QD dimers were prepared from solutions of QDs with diameters ranging from 3.1 to 7.8 nm. Analysis of TEM images confirms that dimer formation involves complete fusion of QD monomers with single grain lattice reconstruction as can be seen in Figure 2. Figure 2a shows a low-resolution TEM image

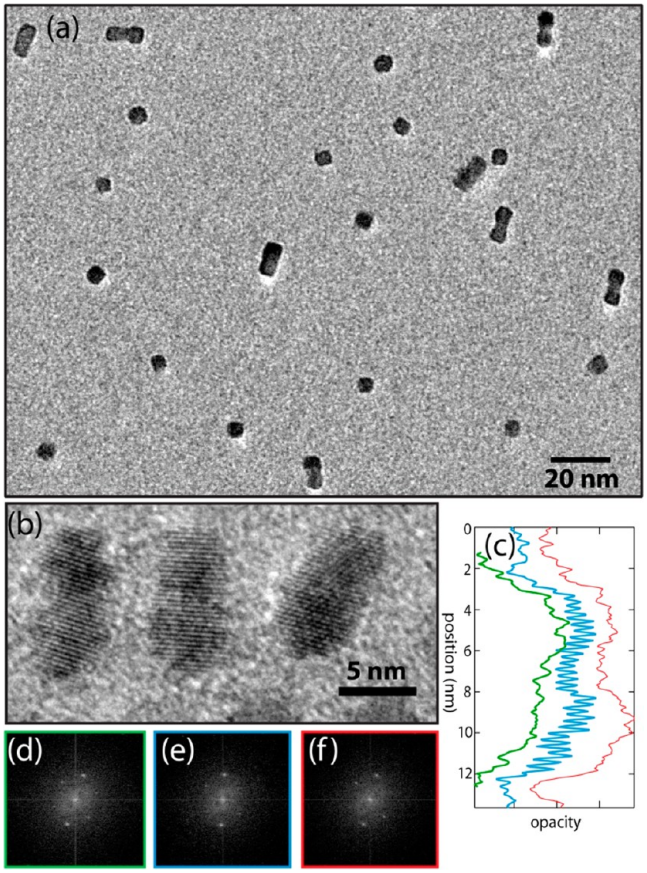

Figure 2. (a) Dimers of PbSe prepared from 7.8 nm quantum dots in the presence of excess oleic acid. (b) TEM image showing three adjacent dimers in an optimized dimerization reaction with high dimer yield. For each dimer, the FFT (d–f) is displayed directly below the TEM. In each FFT image, a pattern of six single spots are seen rather than pairs of spots, indicating that the dimers are oriented into single grained structures. (c) Vertical linescans across the three QD dimers in panel b show the that each dimer retains some of the QD-monomer shape characteristics (e.g., the narrow "waist" in the middle of each line scan). The *z*-contrast linescane analysis relies on the fact that the dimers are single crystals such that the only source of contrast across the crystal is due to thickness variation.

in which a dilute concentration of the product is dispersed on the TEM grid for analysis of the dimer yield. High-resolution images (Figure 2b) show lattice planes that are continuous through the entire structure, and a fast Fourier transform (FFT) analysis of the lattice structure of the complete dimer shows sharp spots indicating single crystal dimers. Figure 2c shows linescans of the opacity along the long axis of the crystals in Figure 2b. The transmission density along the axis still shows character of the monomer subunits where a dip in the opacity can be seen around position 7 nm corresponding to the size of the starting QD monomer.

Absorbance spectra (Figure 3) for QD-dimer solutions differ markedly from those of as-prepared QDs. In Figure 3a,b, we compare the absorption spectra of four starting QD-monomer sizes to those of the subsequent QD-dimer-containing solutions. The spectra in Figure 3a are normalized at 3.1 eV where the per PbSe formula unit molar extinction is independent of QD size[18−21] or shape, while in Figure 3b, the data are normalized at the peak of the 1S band. After a typical dimer synthesis for QD sizes in the 3−6 nm range, the first exciton peak (1S) envelope red shifts approximately 20−40 nm on average. In addition to the overall red shift, QD-dimer solutions prepared from QD monomers with diameters in the range of 3−6 nm most notably exhibit a shoulder blue-shifted from the 1S peak (see arrows in Figure 3a) that results in an apparent broadening of the 1S peak envelope. For QDs approaching 8 nm, this blue-shifted peak appears only as an apparent broadening of the 1S line shape with an overall blue-shifted peak in contrast to the red-shifted peaks for the smaller QD monomers. Thus, there is a clear trend as a function of size; for the smallest sizes, there is a large red shift that decreases with increasing size, and finally there is a blue shift for the largest sizes. These spectral changes are explained below and are related to the size-dependent splitting of the 1S band.

We find that QD-dimer product increases with increasing size of the starting QD monomer, for particles synthesized with an excess of oleic acid. Figure 3c shows the percentage of the solution that is identified as QD dimers as quantified by extensive TEM analysis from reactions using QD monomers with starting diameters of 5.1, 5.9, and 7.8 nm. Dimer percentages were determined by counting QD-dimer populations versus other reaction products over at least 20 TEM images taken at random and counting of at least 30 nanostructures per image to give an unbiased account (see Supporting Information for sample TEM). Upon heating at 150 °C in excess oleic acid, QD-monomer reactants of 5.1, 5.9, and 7.8 nm diameter gave dimer percentages of 17%, 23%, and 34%, respectively.

Dimer formation is sensitive to both reaction time and temperature, with higher occurrences of large QD polymeric chains found after higher temperatures and longer heating intervals. In addition to temperature and reaction time, the initial concentration of QD monomers appears to play a role in the ratio of QD dimers to larger QD oligomeric material. In the typical dimer reaction discussed above, 50 mg of QDs is dissolved in 5 mL of 1-octadecene and then heated. However, when the QD monomer mass is reduced to 10 mg, an increase of about 6% is observed in dimer concentrations for reactions with 5.1 nm QD monomers. The increase in yield can likely be attributed to the inhibition of formation of large PbSe QD oligomer chains by reducing particle−particle interactions, which make QD−QD fusions less probable. In this case, single fusion events become more likely relative to multiple fusion events, thus resulting in higher dimer yields and lower yields of extended-chain species.

SPECTRAL DECOMPOSITION OF DIMER-CONTAINING SAMPLES

In Figure 4, we display the absorbance spectra of QD-dimer solutions that have been prepared from 5.1 nm QD monomers where the oleic acid concentration was varied during synthesis to produce QD dimers that are 21%, 25%, and 31% of the final product. In Figure 4a, the absorbance has been normalized at high photon energy so that changes in the ground state absorption band can be quantitatively analyzed.[18,21] We find that the integrated area of the ground state band remains equivalent for the four spectra shown in Figure 4a, indicating

dx.doi.org/10.1021/ja413026h | J. Am. Chem. Soc. 2014, 136, 4670−4679

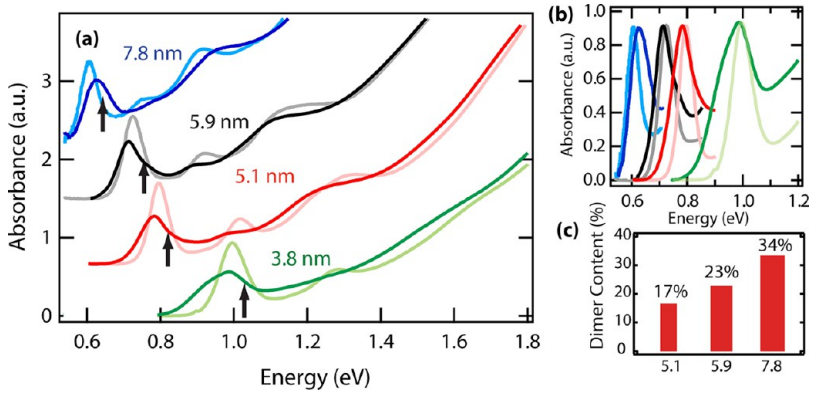

Figure 3. Absorbance spectra for 3.8, 5.1, 5.9, and 7.8 nm QDs (shaded lines) and their corresponding dimer spectra (solid lines), showing characteristic broadening of the ground state peak and the appearance of a shoulder feature blue-shifted from the monomer peak (black arrow). Each spectrum is normalized at 3.1 eV. (b) The same spectra in panel a where the dimer and monomer spectra are normalized at the ground state peak. (c) Dimer concentration as a function of the QD monomer size as determined by analysis of TEM images for the 5.1, 5.8, and 7.8 nm samples.

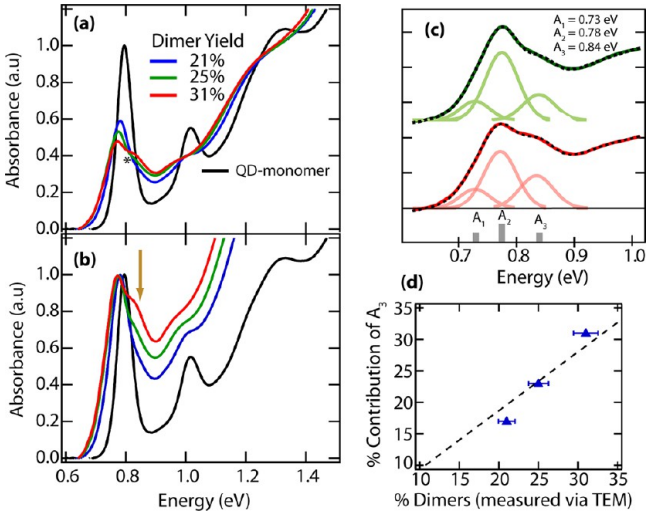

Figure 4. Absorbance spectra of PbSe QD-dimer-containing solutions synthesized from 5.1 nm QD monomers in oleic acid showing the intensity change in the characteristic blue-shifted shoulder as dimer yield increases. In part a, spectra are normalized at high energy (3.1 eV) where absorption per PbSe formula unit absorption is independent of size or shape (∗ denotes isosbestic point). In part b, spectra are normalized at the first exciton peak. Part c shows the spectral decomposition of the ground state peak for the 31% and 25% samples shown in part a. The ground state is decomposed into three Gaussian peaks labeled here as A_1, A_2, and A_3. The dashed green lines show the contribution of each peak to the 25% spectra while the pink lines are for the 31% data. The major change in moving from 25% to 31% dimers is a reduced contribution from A_2 and an increased contribution from A_3. Part d shows total contribution of A_3 to the ground state band as a function of dimer concentration.

that the oscillator strength of the total ground state level is preserved for these samples.[21] For comparison, we show in Figure 4b the data normalized at the peak of the ground state band. In both parts a and b of Figure 4, the black trace is the unreacted QD monomer spectrum. We conclude that the absorption spectra contain contributions mainly from the unreacted QD monomers and the QD dimers from the following evidence: (1) TEM pictographs indicate that there are less than 5% larger QD oligomeric material; (2) a clear isosbestic point at around 0.82 eV (best seen in Figure 4a) results from a decrease in the QD monomer population concurrent with an increase in the QD dimer population. In addition, the presence of the isosbestic point indicates that QD monomers and QD dimers have distinct spectral features.

Spectral decomposition of the ground state band indicates that the dimer-containing spectra contain three peaks, which we have labeled as A_1, A_2, and A_3, for the low-, middle-, and high-energy peaks. In Figure 4c, we show the spectral decomposition for the samples containing 25% (green lines) and 31% (pink lines) QD dimers shown in Figure 4a. A_2 arises from unreacted QD monomers, and its energetic position (0.78 eV) is roughly equal to that of the original QD monomers (0.79 eV). Our data is consistent with a splitting of the ground state band into two peaks for the QD dimer spectra. A_1 and A_3 arise from QD dimers and are equally shifted ±50−60 meV from the QD monomer peak. Figure 4d displays the contribution of the A_3 peak to the total absorbance of the ground state band plotted against the percentage of dimers determined via TEM analysis, indicating that the intensity of A_3 is directly related to the relative concentration of QD dimers to QD monomers.

Photoluminescence measurements of QD dimer solutions confirm our peak assignments. Figure 5 shows the emission from two different QD dimer solutions. In contrast to the absorption band, the emission band consists of only two peaks, one from each of the major species in solution. As in the case of the absorption spectra, we labeled the two emission bands as E_1 and E_2 corresponding to the low- and high-energy bands. The dimers (E_1) only emit from the lowest energy transition corresponding to the A_1 band (see Figure 5b, inset) while the QD monomers emit at E_2 corresponding to the A_2 band. The splitting of the emission and absorbance bands are approximately the same. For example, in Figure 5a, the absorbance bands show a splitting of 50−60 meV, while the shift in emission between E_1 and E_2 is 60 meV. The Stokes shift associated with QD monomers and QD dimers also appears roughly the same.

We analyzed the spectra of QD dimer solutions produced from seven distinct starting QD monomer sizes, ranging from 3.1 to 7.2 nm. Figure 6a displays the spectra near the ground state band for the various sizes, and in Figure 6b, we plot the measured splitting as a function of QD diameter. The splitting ranges from ∼140 meV for the 3.1 nm to ∼50 meV for the largest 7.2 nm QD monomers. At larger QD diameters, the splitting approaches the 35−40 meV inhomogeneous broadening of the ground state exciton envelope induced by the ∼5%

dx.doi.org/10.1021/ja413026h | J. Am. Chem. Soc. 2014, 136, 4670−4679

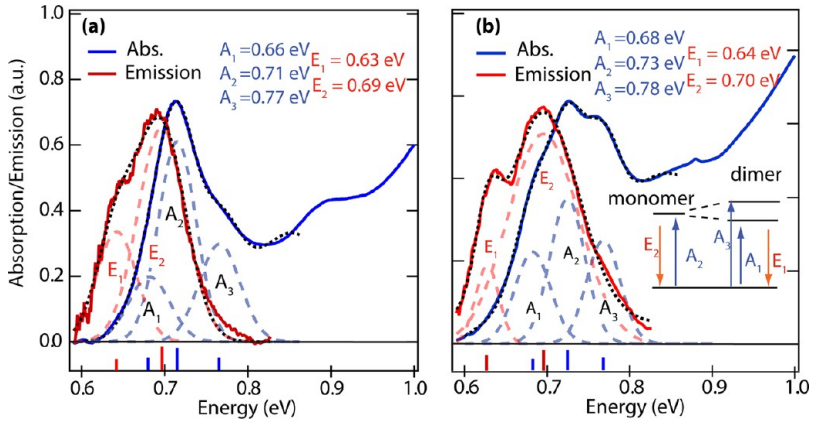

Figure 5. Absorbance spectra (blue) and emission spectra (red) of dimer-containing solutions prepared from (a) 6 nm PbSe QDs monomers and (b) 5.8 nm PbSe monomers (both with oleic acid as the ligand). Absorbance spectra show three absorbance peaks, while emission spectra display two. A simplified level diagram is shown in the inset of part b.

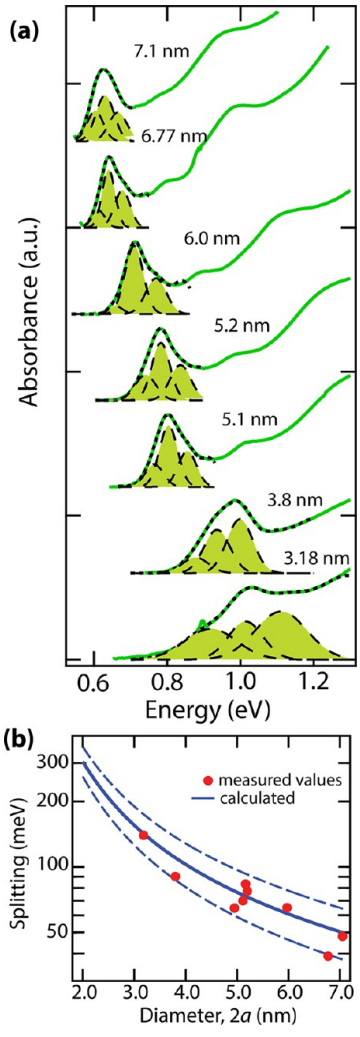

Figure 6. (a) Absorption near the ground state band for seven different QD dimer solutions, offset for clarity. The dashed black trace is the spectral deconvolution. (b) Experimental and theoretical fitted splittings as a function of diameter ($2a$). The dashed curves show predicted splittings for values of the overlap (d) varying by ±15% about the best-fit value.

QD monomer size dispersion. Thus, the larger dimers (greater than ~8 nm) show only a broadened ground state band compared with the more distinct features in the smaller QDs. A similar splitting to what we observe here was found in the optical spectra of coupled GaSb nanoparticle aggregates.[22]

CALCULATION OF GROUND-STATE LEVEL SPLITTING

To analyze theoretically the splitting of the ground-state band, we assume that the individual QDs are faceted polyhedra and that a dimer consists of two identical QDs fused together on equivalent facets. Thus, the geometry of a QD dimer is entirely specified by the polyhedron shape and the orientation of the fused facet. We further assume that the electronic coupling between the wave functions of the individual QDs is weak. Hence the splitting, ΔE, is simply the energy difference between the symmetric and antisymmetric combinations of the wave functions of the individual QDs. We are particularly interested in understanding how ΔE behaves as a function of the distance, b, between the centers of the two QDs with the same size.

Figure 7a shows schematically the oriented attachment of two faceted QDs. For visual simplicity, this figure shows each faceted QD as a simple cube, but this need not be true in general. To determine the wave function, $\psi(r)$, of the individual QDs we make the usual spherical approximation and represent the faceted QD by a sphere of the same volume. For spherical PbSe QDs, the dependence of the wave functions, $\psi(r)$, and the ground-state energy levels, E_0, on the QD radius, a, and confining carrier potential barrier, U_0, were reported in ref 23. These wave functions allow us to calculate the overlap between the wave functions of neighboring QDs. In general, this overlap depends on both a and b. We are mainly interested in the case when the overlap of the two spheres, as characterized by the quantity $d = 2a - b$, is positive and small compared with a. In this limit, the energy splitting is given simply by first-order perturbation theory as

$$\Delta E = 2t_m(U_0, a)\left[1 + \frac{m(U_0 - E_0)d^2}{\hbar^2}\right] \quad (1)$$

where m is the free electron mass and $t_m(U_0,a)$ is the overlap integral between the wave functions on two QDs in exact touching contact.[23] The overlap integral increases with decreasing a and with decreasing U_0 as shown in ref 23.

dx.doi.org/10.1021/ja413026h | J. Am. Chem. Soc. 2014, 136, 4670−4679

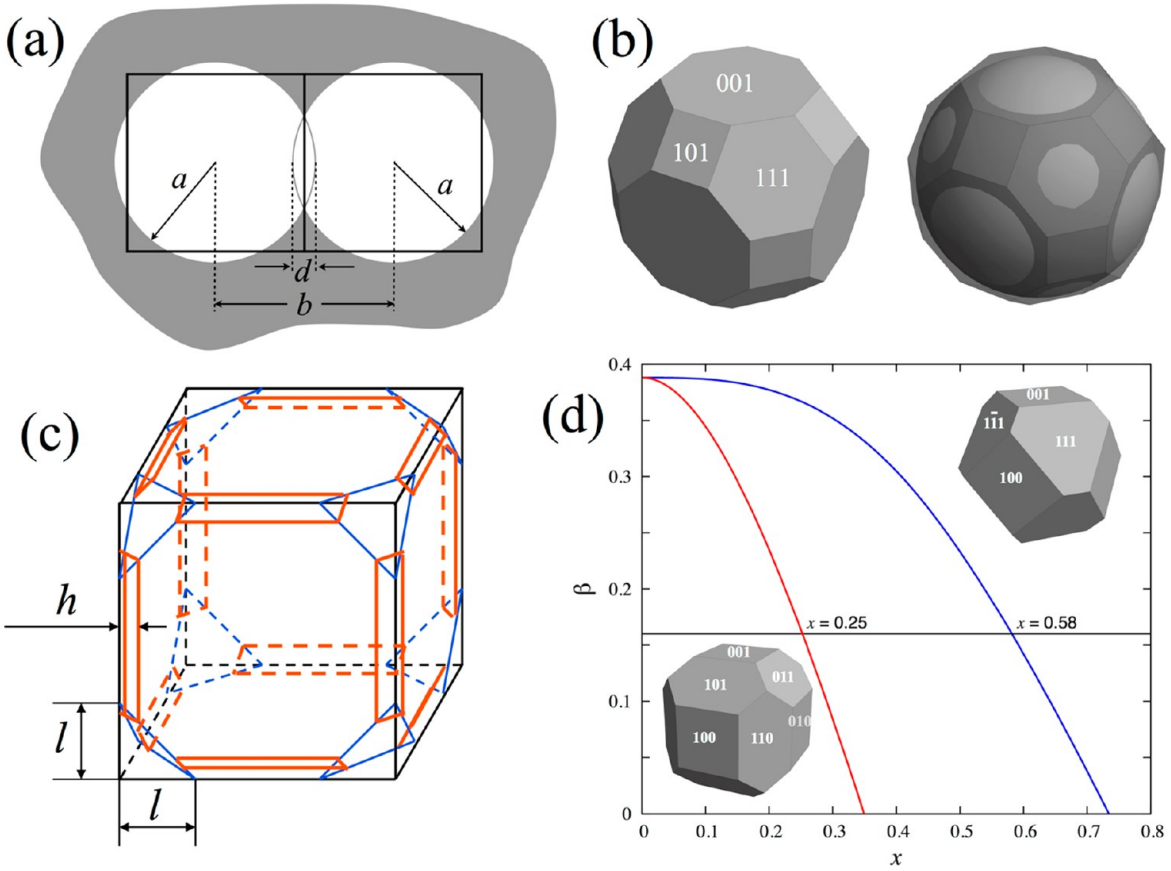

Figure 7. (a) Schematic representation of two QDs, each with the shape of a cube, fused to form a QD dimer. The two QDs can be approximated by spheres having the same volume. The spheres have radius a and separation b between their centers. The width of the overlap volume common to the two spheres is denoted by d. (b) More realistic faceted QD superimposed with a sphere of the same volume. (c) Cube with edges truncated at distance h from the cube vertex, or corners truncated at distance l. Truncating the cube along the edges results in {110} facets while truncating at the corners results in {111} facets. (d) Variation in the proportionality constant β (see text) for the two cases: truncated edges (red, $x = h/(2a)$) and truncated corners (blue, $x = l/(2a)$). Two shapes that are consistent with the experimentally determined value of β are shown.

The overlap, d, corresponds geometrically to the lens-shaped volume shown in Figure 7a. For the simple case of a cubic QD, d is proportional to the radius of the sphere: $d = [2 - (4\pi/3)^{1/3}]a \approx 0.39a$. For QDs with more realistic polyhedral shapes [Figure 7b], the sphere extends outside some facets. If the two QDs are attached at these facets then the thickness d of the overlap region again varies linearly with the radius a of the sphere, but the proportionality constant will now depend on the detailed shape of QD and the direction of contacting facets. Hence we write the general dependence of d on a as

$$d = \beta a + \gamma \tag{2}$$

We expect the geometrical factor β always to be less than its cubic limiting value of 0.39. The offset γ represents a correction to pure proportionality and is expected to be small compared with d.

Experimentally, the splitting of the band edge absorption line decreases with the QD radius [cf. Figure 6b]. Equation 1 shows that this splitting depends on U_0, a, and d. It is reasonable to assume that U_0 is the same for all PbSe QDs regardless of their size and shape. Hence, we can attribute the experimental dependence of the splitting on the radius entirely to a and d. Our goal is to use the observed splittings to derive information about the QD shapes that are consistent with eqs 1 and 2. Thus, we insert eq 2 into eq 1 and use the resulting expression to model the observed splittings in Figure 6a. We take the depth of the potential well to be constant, $U_0 = 1.0$ eV.

The fit is shown in Figure 6b and gives $\beta = 0.16 \pm 0.03$ and $\gamma = 0.24 \pm 0.09$ nm. As expected, the proportionality constant β is substantially less than the value obtained for perfect cubes because most QDs have {110} or {111} facets or both, which makes them closer to spherical. The intercept γ has the scale of an interatomic distance and is indeed small compared with typical values of d. Physically, it represents the slight increase in the QD effective radius arising from atomic-scale roughness of the surface facets. The statistical uncertainty in γ is less than 1 Å and is therefore insignificant compared with the QD size. Variations of 0.2 eV in the value of U_0 have a negligible effect on the value of β, and the intercept γ varies by only 0.03 nm.

Figure 6b shows that while the overall dependence of the splitting on the QD size is nicely explained by our geometrical model, there are fluctuations around the solid curve (corresponding to $\beta = 0.16$). We attribute these to variations in the QD shapes, which give rise to variations in β. The dashed curves in Figure 6b, which encompass the observed fluctuations, correspond to variations in β of ±15%. These shape variations lead to broadening of the peaks in the absorption and emission spectra that are associated with the split energy level of the QD ground state. Indeed, this additional broadening of the A_1 and A_3 peaks and dimer PL line is seen in Figures 5 and 6.

dx.doi.org/10.1021/ja413026h | J. Am. Chem. Soc. 2014, 136, 4670−4679

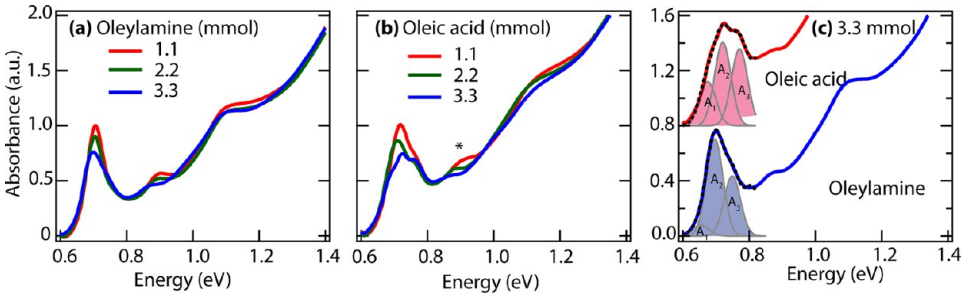

Figure 8. Absorbance spectra for dimers prepared in (a) oleylamine and (b) oleic acid as a function of ligand concentration (asterisk denotes the P-exciton). Spectra are normalized at 3.1 eV. In part c, the spectral decomposition is shown for 3.3 mmol case of oleic acid (red) and oleylamine (blue).

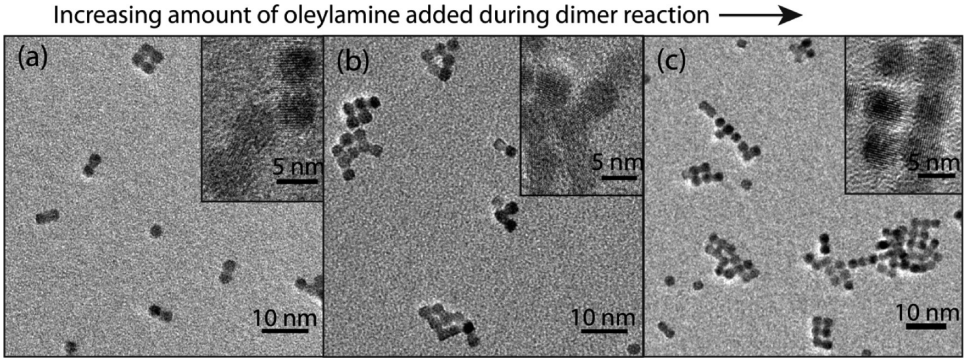

Figure 9. Increasing the amount of oleylamine (rather than oleic acid) from 1.1 to 2.2 and 3.3 mmol (a–c, respectively) produces progressively larger oligomers, rather than the desired increase in dimer structures, similar to that found following pyridine exposure.[14] The inset of each panel shows high resolution lattice alignment showing that with oleylamine the assemblies often form in a multicrystalline manner.

■ DETERMINING QD SHAPE AND MORPHOLOGY

The shape of a fully faceted QD can be completely specified by the relative surface area of each facet. For QDs that maintain their equilibrium crystal shape, these surface areas depend on the surface energies of the different facets,[24] but in general, other factors may influence or determine the QD shape. For simplicity, it is convenient to approximate faceted PbSe QDs as truncated cubes with {100}, {110}, and {111} facets and full octahedral (O_h) symmetry (Figure 7c).

The proportionality constant, $\beta = 0.16$, obtained from fitting the experimental splittings imposes restrictions on the possible shapes of the individual QDs. We consider the two simplified limiting cases illustrated schematically in Figure 7c: a cube with either truncated edges (red outline showing truncation by h) or truncated corners (blue outline showing truncation by l). Figure 7d shows how β depends on h and l, here represented by relative values $x = h/(2a)$ (red trace) and $x = l/(2a)$ (blue trace). For the case of truncated edges, $\beta = 0.16$ corresponds to $x = 0.25$. For the case of truncated corners, $\beta = 0.16$ corresponds to $x = 0.58$. These two polyhedron shapes are shown by the insets. Although they are qualitatively quite different, the relative fraction of the total surface area having {001} orientation is roughly comparable: 65% for the cube with truncated edges and 40% for the cube with truncated corners. For cases that have both truncated edges and truncated corners, we expect this fractional area to have values lying within this range.

■ LIGAND VARIATION

Varying the type of ligand and the ligand concentration has marked effects on QD dimer yield. For a sample of 5.9 nm QD monomers, we performed a side-by-side comparison of oleylamine (Figure 8a) and oleic acid (Figure 8b) varying the amount of each ligand from 1.1 to 3.3 mmol. For both ligands, the appearance of the A_3 peak increases with increasing ligand concentration, although some striking differences are observed.

Upon increase of the oleylamine concentration, the 1S peaks shift to lower energies than those in the oleic acid samples. Additionally, the appearance of the blue-shifted shoulder with increasing oleylamine concentration is less pronounced. From TEM image analysis (Figure 9), the greatest point of contrast between the reaction products for these two samples is in the percentage of larger QD oligomeric material. While the percent oligomeric material ranges from 1% to 5% for the oleic acid-containing samples, samples using oleylamine produced as much as 44% QD oligomeric material with 3.3 mmol of oleylamine as shown in Figure 9. This observation is consistent with that of Hanrath et al.[14] who exposed PbSe QD solutions to pyridine and observed mainly the formation of polymeric PbSe QD networks. The largest oligomers are observed in samples containing the highest concentrations of oleylamine, as shown in Figure 9. Furthermore, QD dimer and QD oligomer fusion using oleic acid proceeds via oriented attachment predominantly along the {100} facets. In contrast, fusion in the presence of oleylamine seems to show no preference for specific facets (as shown in Figure 9, high resolution insets).

In addition to the 1S level splitting, we observe a shift to lower energies (relative to the 1S level) of the 1P band as the dimer population increases (see asterisk in Figure 8b). The second exciton results from splitting of the (3×8) degenerate 1P states into $1P_{1/2}$ and a $1P_{3/2}$ due to the band anisotropy[25,26] and mixing of interband valence states.[27] These states are likely further split by the wave function overlap described above.

dx.doi.org/10.1021/ja413026h | J. Am. Chem. Soc. 2014, 136, 4670–4679

At this stage, we have not yet optimized the synthetic conditions to achieve quantitative QD dimer yields. We have begun preliminary explorations of separation techniques to further isolate the desired QD dimer species. Initially we attempted size-selective precipitation of reaction products using hexane/ethanol as the solvent/nonsolvent pair and were successful at removing some of the largest QD oligomers, though it did not efficiently resolve QD monomer and QD dimer species. Other harsher techniques such as ultracentrifugation using organic density gradients[28] resulted in sample degradation.

MECHANISTIC ROLE OF EXCESS LIGAND

The significant increase in QD oligomeric material observed when excess oleylamine is employed in lieu of oleic acid suggests possible mechanisms for the role of excess capping reagent in QD dimer formation. Long-chain hydrocarbons with Lewis basic functional head groups are typically employed as surface stabilizers for Pb-chalcogenide QDs. These Lewis bases bind to surface Pb atoms, resulting in bonds with varying degrees of polarity, depending on the nature of the functional headgroup and exposed crystal facets. Interactions between surface cations (Lewis acids) and stabilizing ligands (Lewis bases) can be characterized in terms of hard and soft acid/base interactions (HSAB). According to HSAB, hard acids and bases are compact and nonpolarizable while soft acids and bases are larger and more diffuse due to inner electrons shielding nuclear charge from the outer electrons making them more polarizable. The most stable adducts are formed from hard–hard and soft–soft interactions. Typical surface ligands for the Pb-chalcogenides include carboxylic acids($R\text{-}CO_2^-$), thiolates (RS^-), amines (RNH_2), and phosphonates ($R\text{-}PO_3H^{2-}$). The approximate order of increasing hardness of these ligands as Lewis bases follows the trend $RS^- > RNH_2 > R\text{-}CO_2^- \approx R\text{-}PO_3H_2$, while Pb^{2+} is a relatively soft acid. Following this line of reasoning, soft to intermediate base-containing ligands such as oleylamine should form the most stable bond with the Pb^{2+} orbital at the PbSe QD surface. These interactions should in part explain the comparative differences in the occurrence of oriented attachment in samples containing oleic acid and oleylamine.

Given the structural nature of PbSe QDs as multifaceted crystals with a stoichiometric core and a terminating surface shell of surfactant-stabilized Pb atoms, the role of excess ligand may more accurately be described as one of removing or etching Pb atoms from the QD surface. Moreels et al. observed that during storage of oleic acid-capped QDs under ambient conditions, some of the oleic acid ligands desorbed surface Pb to form an equilibrium between bound ligands and free $Pb(oleate)_2$ in solution.[29] As the free oleic acid concentration is increased, so too is the amount of desorbed Pb^{2+} forming additional free $Pb(oleate)_2$. Given that oleylamine should form a bond with Pb^{2+} that is covalent in nature involving lone pairs on the N atom, we expect excess oleylamine to be at least as effective as oleate at stripping away surface Pb atoms, when present in excess, and exposing unpassivated surfaces. These bare surface sites are then less sterically hindered from undergoing fusion and attach more efficiently. Fusion may also be driven by the need to decrease the surface energies of these bare surface sites. A second case to consider is that amines may not exhibit tight binding to all of the crystal facets of PbSe. Cho et al. observe that addition of oleylamine to the PbSe reaction mixture induces the formation of octahedral PbSe nanoparticles.[1] This evidence suggests that oleylamine binds more efficiently to the {111} facets, which allows for faster growth of the {100} facets. Therefore, it is likely that oleylamine is very effective at removing Pb^{2+} from surfaces where tight binding occurs (like the {111}) and is in dynamic equilibrium undergoing exchange more readily at other surfaces (like the {100}). This dual interaction thus explains why oriented attachment is so efficient in reactions containing excess oleylamine giving rise to uncontrolled QD oligomeric samples.

Carboxylate, a hard acid, should form a more polar bond with surface Pb atoms. Given an excess of oleic acid, a protonated carboxylate, extraction of Pb must occur through a proton exchange at the surface. A possible mechanism for Pb extraction is one of $Pb(oleate)_2$ leaving behind a proton in the vacant Pb site at the QD surface. This process, like in the case of oleylamine, requires the breaking of a covalent Pb–Se bond, but now a proton transfer must occur to the PbSe surface to make a stable $Pb(oleate)_2$ molecule. Thus, unlike amines that undergo fast exchange at the {100} surface, oleic acid must exhibit some kinetic hindrance to fusion associated with the proton transfer.

In addition to oleylamine, $Pb(oleate)_2$ was employed in the reaction in lieu of oleic acid. The absorbance spectra of 7.8 nm QDs reacted in the presence of lead oleate (Figure 10) reveal a much narrower 1S peak compared with the QD monomers (Figure 10, green trace) and QD dimers (Figure 10, red trace), indicating a decrease in the size dispersion and a slight red-shift of the 1S band. A TEM analysis (not shown) supported this decrease in size dispersion. The red shift observed upon addition of $Pb(oleate)_2$ is consistent with addition of Pb atoms to the QD surface. In previous work, we also observed a red shift when Se was added to the QD surface.[5] The difference in interaction for $Pb(oleate)_2$ reactions, compared with oleic acid-containing reactions, is 2-fold. First, by addition of $Pb(oleate)_2$, in which there is presumably only a small excess of free oleic acid molecules, there is less free ligand available to extract Pb at the QD surface. Second, it is now possible that the excess $Pb(oleate)_2$ molecules bind to the PbSe {100} facets either through chemisorption or physisorption to surface Se atoms offering some steric hindrance, which impedes the occurrence of oriented attachment. This experiment directly supports our ligand concentration-dependent QD dimer formation studies, which show that higher concentrations of free ligand present in the reaction mixture resulted in greater dimer yields.

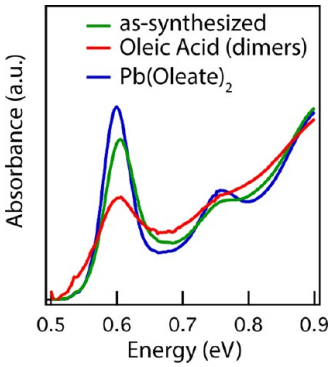

Figure 10. Absorbance spectra for dimers prepared from 7.8 nm quantum dots in the presence of either oleic acid or $Pb(oleate)_2$.

dx.doi.org/10.1021/ja413026h | J. Am. Chem. Soc. 2014, 136, 4670–4679

If QD-dimer formation is viewed in light of this picture of exposed or ligand-free surfaces fusing, then our size-dependent QD dimer formation trends in the presence excess oleic acid also make sense. PbSe QDs are best modeled as truncated octahedra with six stoichiometric 100 facets and eight high energy {111} facets that undergo surface-atom rearrangements to lower surface energies and leave the facet Pb-terminated.[10] Importantly, different ligands are known to exhibit facet-specific binding affinities[1] to PbSe, and oleate-capped QDs are observed to fuse primarily along the {100} faces. This leaves two possible mechanisms for QD−ligand interactions for oleate capped PbSe: (1) oleate does not sufficiently passivate the {100} facets of PbSe, or (2) oleate ligands are efficiently removing excess Pb atoms from the {100} surfaces. In both cases, a larger {100} surface area would lend itself to greater occurrences of oriented attachment of monomer particles for reactions containing oleic acid.

CONCLUSIONS

We have demonstrated that various synthetic parameters can be tuned to affect the QD dimer yield in a novel oriented attachment reaction. We achieved QD dimer yields approaching ∼50% starting from monodisperse QD monomer solutions resulting in dimer concentrations of ∼40%. We showed that the dimer yield is dependent on QD size and excess stabilizing ligand. In addition to PbSe QD homodimers (dimers composed of the same size and material), PbSe QD heterostructures were also prepared using 4.6 and 7.8 nm PbSe QDs (Figure 11). Though successful fusion of large and small QDs was achieved, yields for PbSe heterodimers were very low, giving only ∼10% heterostructured products.

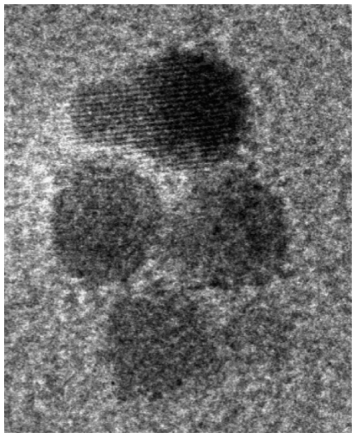

Figure 11. TEM showing PbSe heterodimers.

Our results have demonstrated a different approach toward producing anisotropic PbSe nanostructures, and they utilize the notion that the QDs can be used as reagents to produce more complex nanostructures. The optical spectra of the dimers show the splitting of the ground exciton states connected with a creation of symmetric and antisymmetric superposition of electron and hole states in two adjacent QDs. We describe this splitting within spherical approximation model assuming that the dimers are formed as a result of oriented attachment of two QDs, which are fused primarily along the {100} faces. Our results should have implications toward rational bottom-up approaches to nanostructure synthesis.

ASSOCIATED CONTENT

Supporting Information

Description of the synthesis of the starting QD monomers and example TEM for counting dimer yield. This material is available free of charge via the Internet at http://pubs.acs.org.

AUTHOR INFORMATION

Corresponding Author

matt.beard@nrel.gov

Notes

The authors declare no competing financial interest.

ACKNOWLEDGMENTS

We thank M. Law for help on the initial stages of this project and Geoff Diederich for synthesis of one sample. We thank Steve Hughes for helpful discussions. B.K.H, J.L.B., J.M.L., D.K., and M.C.B. acknowledge support from the Solar Photochemistry program within the division of Chemical Sciences, Geosciences, and Biosciences, Office of Science, Office of Basic Energy Sciences (BES), funded by the Department of Energy (DOE). DOE funding to NREL was provided through Contract DE-AC36-08GO28308. A.S. acknowledges support of the Center for Advanced Solar Photophysics (CASP), an Energy Frontier Research Center founded by Office of Basic Energy Sciences (BES), Office of Science, the Department of Energy (DOE). A.L.E. and S.C.E. acknowledge financial support of the Office of Naval Research (ONR) through the Naval Research Laboratory's Basic Research Program.

REFERENCES

(1) Cho, K.-S.; Talapin, D. V.; Gaschler, W.; Murray, C. B. *J. Am. Chem. Soc.* **2005**, *127*, 7140.
(2) Evers, W. H.; Goris, B.; Bals, S.; Casavola, M.; de Graaf, J.; Roij, R. v.; Dijkstra, M.; Vanmaekelbergh, D. *Nano Lett.* **2013**, *13*, 2317.
(3) Schliehe, C.; Juarez, B. H.; Pelletier, M.; Jander, S.; Greshnykh, D.; Nagel, M.; Meyer, A.; Foerster, S.; Kornowski, A.; Klinke, C.; Weller, H. *Science* **2010**, *329*, 550.
(4) Querejeta-Fernandez, A.; Hernandez-Garrido, J. C.; Yang, H. X.; Zhou, Y. L.; Varela, A.; Parras, M.; Calvino-Gamez, J. J.; Gonzalez-Calbet, J. M.; Green, P. F.; Kotov, N. A. *ACS Nano* **2012**, *6*, 3800.
(5) Hughes, B. K.; Ruddy, D. A.; Blackburn, J. L.; Smith, D. K.; Bergren, M. R.; Nozik, A. J.; Johnson, J. C.; Beard, M. C. *ACS Nano* **2012**, *6*, 5498.
(6) Smith, D. K.; Luther, J. M.; Semonin, O. E.; Nozik, A. J.; Beard, M. C. *ACS Nano* **2011**, *5*, 183.
(7) Semonin, O. E.; Luther, J. M.; Beard, M. C. *Mater. Today* **2012**, *15*, 508.
(8) Stewart, J. T.; Padilha, L. A.; Midgett, A. G.; Qazilbash, M. M.; Pietryga, J. M.; Luther, J. M.; Beard, M. C.; Nozik, A. J.; Klimov, V. I. *Nano Lett.* **2012**, *12*, 622.
(9) Pandey, A.; Guyot-Sionnest, P. *Science* **2008**, *322*, 929.
(10) Fang, C. M.; van Huis, M. A.; Vanmaekelbergh, D.; Zandbergen, H. W. *ACS Nano* **2010**, *4*, 211.
(11) Koh, W.-k.; Bartnik, A. C.; Wise, F. W.; Murray, C. B. *J. Am. Chem. Soc.* **2010**, *132*, 3909.
(12) Schapotschnikow, P.; van Huis, M. A.; Zandbergen, H. W.; Vanmaekelbergh, D.; Vlugt, T. J. H. *Nano Lett.* **2010**, *10*, 3966.
(13) Klokkenburg, M.; Houtepen, A. J.; Koole, R.; de Folter, J. W. J.; Erne, B. H.; van Faassen, E.; Vanmaekelbergh, D. *Nano Lett.* **2007**, *7*, 2931.
(14) Hanrath, T.; Veldman, D.; Choi, J. J.; Christova, C. G.; Wienk, M. M.; Janssen, R. A. J. *ACS Appl. Mater. Interfaces* **2009**, *1*, 244.
(15) Zhang, Q.; Liu, S. J.; Yu, S. H. *J. Mater. Chem.* **2009**, *19*, 191.

(16) Jiang, F.; Li, Y. C.; Ye, M. F.; Fan, L. Z.; Ding, Y. Q.; Li, Y. F. *Chem. Mater.* **2010**, *22*, 4632.
(17) Bilecka, I.; Niederberger, M. *Nanoscale* **2010**, *2*, 1358.
(18) Moreels, I.; Lambert, K.; De Muynck, D.; Vanhaecke, F.; Poelman, D.; Martins, J. C.; Allan, G.; Hens, Z. *Chem. Mater.* **2007**, *19*, 6101.
(19) Klimov, V. I. *J. Phys. Chem. B* **2000**, *104*, 6112.
(20) Yu, W. W.; Qu, L. H.; Guo, W. Z.; Peng, X. G. *Chem. Mater.* **2003**, *15*, 2854.
(21) Yu, P.; Beard, M. C.; Ellingson, R. J.; Ferrere, S.; Curtis, C.; Drexler, J.; Luiszer, F.; Nozik, A. J. *J. Phys. Chem. B* **2005**, *109*, 7084.
(22) Mirafzal, H.; Kelley, D. F. *J. Phys. Chem. C* **2009**, *113*, 7139.
(23) Shabaev, A.; Efros, Al. L.; Efros, A. L. *Nano Lett.* **2013**, *13*, 5454.
(24) Erwin, S. C.; Zu, L. J.; Haftel, M. I.; Efros, A. L.; Kennedy, T. A.; Norris, D. J. *Nature* **2005**, *436*, 91.
(25) Bartnik, A. C.; Efros, A. L.; Koh, W. K.; Murray, C. B.; Wise, F. W. *Phys. Rev. B* **2010**, *82*, No. 195313.
(26) Tudury, G. E.; Marquezini, M. V.; Ferreira, L. G.; Barbosa, L. C.; Cesar, C. L. *Phys. Rev. B* **2000**, *62*, 7357.
(27) An, J. M.; Franceschetti, A.; Dudiy, S. V.; Zunger, A. *Nano Lett.* **2006**, *6*, 2728.
(28) Bai, L.; Ma, X. J.; Liu, J. F.; Sun, X. M.; Zhao, D. Y.; Evans, D. G. *J. Am. Chem. Soc.* **2010**, *132*, 2333.
(29) Moreels, I.; Fritzinger, B.; Martins, J. C.; Hens, Z. *J. Am. Chem. Soc.* **2008**, *130*, 15081.